DEVELOPMENT

A cytoplasmic role of Wnt/β-catenin transcriptional cofactors Bcl9, Bcl9l, and Pygopus in tooth enamel formation

Claudio Cantù,[1]* Pierfrancesco Pagella,[2]* Tania D. Shajiei,[2] Dario Zimmerli,[1] Tomas Valenta,[1] George Hausmann,[1] Konrad Basler,[1†] Thimios A. Mitsiadis[2†]

Wnt-stimulated β-catenin transcriptional regulation is necessary for the development of most organs, including teeth. Bcl9 and Bcl9l are tissue-specific transcriptional cofactors that cooperate with β-catenin. In the nucleus, Bcl9 and Bcl9l simultaneously bind β-catenin and the transcriptional activator Pygo2 to promote the transcription of a subset of Wnt target genes. We showed that Bcl9 and Bcl9l function in the cytoplasm during tooth enamel formation in a manner that is independent of Wnt-stimulated β-catenin–dependent transcription. Bcl9, Bcl9l, and Pygo2 localized mainly to the cytoplasm of the epithelial-derived ameloblasts, the cells responsible for enamel production. In ameloblasts, Bcl9 interacted with proteins involved in enamel formation and proteins involved in exocytosis and vesicular trafficking. Conditional deletion of both Bcl9 and Bcl9l or both Pygo1 and Pygo2 in mice produced teeth with defective enamel that was bright white and deficient in iron, which is reminiscent of human tooth enamel pathologies. Overall, our data revealed that these proteins, originally defined through their function as β-catenin transcriptional cofactors, function in odontogenesis through a previously uncharacterized cytoplasmic mechanism, revealing that they have roles beyond that of transcriptional cofactors.

INTRODUCTION

Wnt signaling plays fundamental roles in virtually all aspects of embryonic development and organogenesis (*1*). Wnt signaling–dependent transcription is mediated by the nuclear accumulation of β-catenin, which binds to transcription factors of the T cell factor/lymphoid enhancer factor (TCF/LEF) family and serves as a scaffold for an ensemble of cofactors, such as Legless (Lgs) and Pygopus (Pygo), which are important for transcriptional activation (*2*). Lgs and Pygo were first identified in *Drosophila melanogaster* as dedicated cofactors of Armadillo, the fly homolog of β-catenin. Mutation of either *lgs* or *pygo* induced a phenotype recapitulating the complete loss of Wnt signaling (*3*, *4*). A "chain of adaptors" model was proposed, in which TCF, β-catenin, Lgs, and Pygo are successively recruited to the DNA to activate Wnt target gene expression (*5*–*7*). In this model, the only function of Lgs is to recruit Pygo to β-catenin. However, mutations in the genes encoding homologs of Pygo (*Pygo1* and *Pygo2*, hereafter referred to as *Pygo1/2*) and Lgs (*Bcl9* and *Bcl9l*, referred to as *Bcl9/9l*) in the mouse revealed that their loss-of-function phenotype does not always recapitulate the effects of Wnt/β-catenin loss (*8*–*10*). These proteins are therefore considered to be tissue-specific β-catenin transcriptional effectors (*8*, *10*).

Tooth development is critically dependent on the Wnt/β-catenin pathway (*11*–*13*). Wnt ligands are produced in developing teeth, and loss of β-catenin leads to the arrest of odontogenesis at early stages (*11*). Teeth develop as a result of sequential and reciprocal interactions between cells of the oral epithelium and mesenchymal cells derived from the cranial neural crest (*14*). Odontogenesis in both rodents and humans proceeds through a series of well-defined morphological stages, namely, the bud, cap, bell, and differentiation and mineralization stages (*14*). Differentiation of mesenchymal cells gives rise to the dentin-producing odontoblasts, whereas the enamel-forming ameloblasts originate from epithelial cells (*14*). In contrast to molars, rodent incisors are continuously growing organs with anatomically distinct and molecularly defined territories, where cell proliferation, differentiation, and maturation events can be easily analyzed. A pool of dental epithelial stem cells located in the proximal part of the incisor (the labial cervical loop) ensures the constant generation of ameloblasts. These cells produce new enamel to compensate for hard tissue loss resulting from mastication. Wnt/β-catenin signaling is a key regulator of incisor epithelial stem cell homeostasis (*13*).

Here, we investigated the role of Bcl9/9l and Pygo1/2 during tooth formation and homeostasis using the mouse incisor as a model system. We found that Bcl9/9l and Pygo1/2 were strictly required for amelogenesis (the formation of enamel) and acted independently of the Wnt/β-catenin pathway. Bcl9/9l and Pygo1/2 functioned in the cytoplasm along the secretory pathway, where they interacted with the enamel-specific protein amelogenin, a crucial actor in amelogenesis. We speculate that Bcl9/9l and Pygo2 might also be key factors important for the secretion of specific proteins in other tissues.

RESULTS

Bcl9/9l and Pygo2 are present in the secretory, differentiated ameloblasts

We first analyzed the distribution of β-catenin, Bcl9, Bcl9l, and Pygo2 in the developing mouse incisor (Fig. 1, A to C) by immunohistochemistry. β-Catenin was detected only in the dental epithelium of the incisor, from the cervical loop, where the stem cells are located, to the most differentiated anterior region, at all the stages analyzed from embryonic day 15.5 (E15.5) to postnatally at day 0 (P0) (Fig. 1, D to F, and fig. S1). Similarly, Bcl9 was present in dental epithelial cells at E15.5 (Fig. 1G) and P0 (Fig. 1H). However, at P0, Bcl9 was restricted to differentiated ameloblasts, where it displayed an asymmetric cytoplasmic distribution, being more abundant in the apical secretory portion of the cells (Fig. 1, H and I, and fig. S1). Bcl9l was present at E15.5 throughout the cytoplasm in both the epithelial and mesenchymal cells (Fig. 1, J to L), but, at P0, its distribution was limited to the dental epithelium.

[1]Institute of Molecular Life Sciences, University of Zurich, 8057 Zurich, Switzerland. [2]Orofacial Development and Regeneration, Institute of Oral Biology, Center of Dental Medicine, University of Zurich, 8032 Zurich, Switzerland.
*These authors contributed equally to this work.
†Corresponding author. Email: konrad.basler@imls.uzh.ch (K.B.); thimios.mitsiadis@zzm.uzh.ch (T.A.M.)

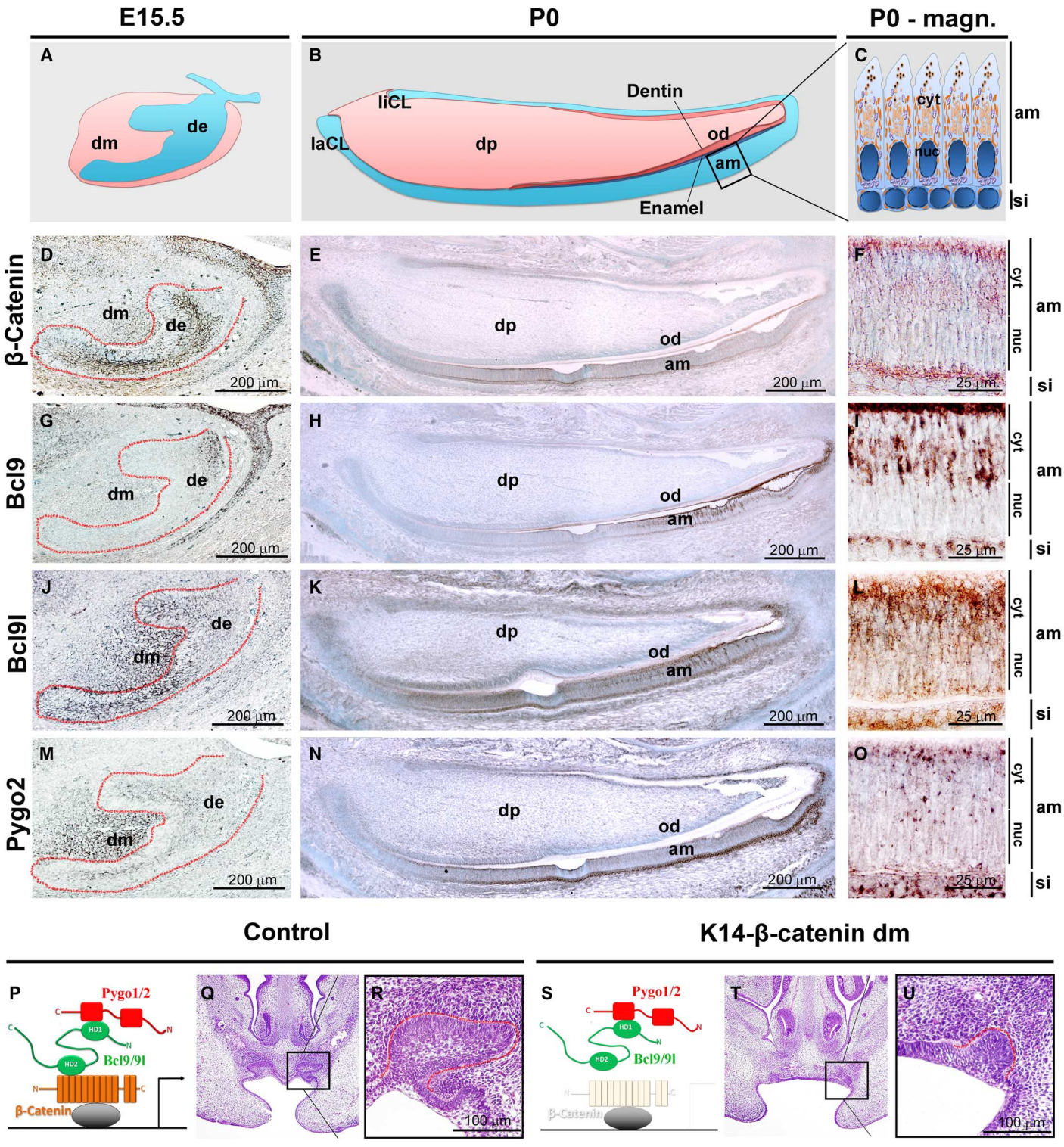

Fig. 1. The β-catenin cofactors Bcl9, Bcl9l, and Pygo2 are present in the developing tooth. Schematic representation of (**A**) a mouse incisor at E15.5 and (**B**) a longitudinal section of a mouse lower incisor at birth (P0). dm, dental mesenchyme; de, dental epithelium; laCL, labial cervical loop; liCL, lingual cervical loop; dp, dental pulp; od, odontoblasts. (**C**) Schematic representation of the differentiated dental epithelium. si, stratum intermedium; cyt, cytoplasm; nuc, nucleus; am, ameloblast. (**D** to **O**) Immunohistochemistry showing the distribution of β-catenin, Bcl9, Bcl9l, and Pygo2 at E15.5 and P0. Each staining shown is representative of at least $n = 3$ individual mice. (**P**) Schematic of the complex formed by Pygo, Bcl9/9l, and β-catenin at a target promoter. The gray oval represents the transcription factor TCF/LEF. (**Q**) Transverse section of hematoxylin and eosin–stained developing wild-type upper incisors at E15.5. (**R**) Higher-magnification view of boxed tooth germ in (Q). When β-catenin–dependent transcription is blocked in K14-Cre-bcat-dm embryos (**S**), early tooth development is arrested (**T** and **U**). $n = 3$.

Similarly, Pygo2 was present at E15.5 in both epithelial and mesenchymal cells (Fig. 1M) but, at P0, was observed only in the cytoplasm of epithelial cells, most notably ameloblasts and the underlying stratum intermedium (Fig. 1, N and O, and fig. S1).

Conditional deletion of β-catenin, but not of Bcl9/9l, leads to arrested tooth development

Epithelium-specific deletion of the gene encoding β-catenin, *Ctnnb1*, using the K14-Cre driver caused tooth development to arrest at E14.5 (*11*). To distinguish between the role of β-catenin as a transcriptional regulator and its role as a key component of adherens junctions, we exploited a β-catenin double-mutant allele (*dm*) (*3*). This allele encodes a transcriptionally nonfunctional protein that fully retains its structural contribution to adherens junctions (*3*). In accordance with previously published results, K14-Cre; $Ctnnb1^{flox/dm}$ mice (K14-β-cat-dm) exhibited arrested incisor development at E14.5 (Fig. 1, P to U, and fig. S2) (*11*).

We then investigated whether the β-catenin transcriptional cofactors Bcl9/9l had similar roles in early stages of odontogenesis. For this purpose, we generated mice lacking Bcl9/9l in the epithelium by combining the K14-Cre driver with LoxP-containing alleles of *Bcl9/9l* (K14-Cre; $Bcl9^{flox/flox}$; $Bcl9l^{flox/flox}$ mice, referred to as K14-Bcl9/9l-flox) (*15*). In contrast to the phenotype caused by loss of β-catenin–dependent transcription (K14-β-cat-dm), incisors fully developed in the *Bcl9/9l* mutant mice (fig. S3). However, these incisors did not have the red-yellow pigmentation that is characteristic of wild-type mouse incisors (K14-Bcl9/9l-control; Fig. 2, A and B), but instead have a white appearance (Fig. 2, C and D). These results suggest that Bcl9/9l affect the production and composition of the enamel.

Bcl9/9l and Pygo1/2 act independently of β-catenin to ensure proper enamel formation

Enamel is the hardest mineralized tissue in vertebrates and is characterized by a highly organized structure that is necessary for its exceptional hardness and durability. We used scanning electron microscopy (SEM) to investigate possible defects in the structural organization of the enamel in *Bcl9/9l* mutant mice. Mutant teeth showed a disorganized structure of the enamel, notably abnormalities in the orientation, arrangement, and thickness of the enamel rods (Fig. 2, E to H). The white and glossy appearance of the incisors in K14-Bcl9/9l-flox mutants additionally suggests lack of iron, an element that increases the hardness of enamel in rodents and contributes to enamel color (*16*). We used energy-dispersive x-ray spectroscopy (EDS) to quantify the relative abundance of iron and other elements, such as magnesium (Mg^{2+}) and calcium (Ca^{2+}), throughout the enamel. EDS showed that iron was enriched at the enamel surface and accounted for about 4% of total enamel mass (Fig. 2I) in incisors from wild-type mice. In contrast, the enamel of incisors from K14-Bcl9/9l-flox mice contained less iron (0.5% of its total mass; Fig. 2J). The relative abundance of all other elements was not affected in the enamel of the mutant incisors (Fig. 2, I and J). Consistent with the observed iron loss and the important role of iron in enamel hardness, incisors of K14-Bcl9/9l-flox mutants showed deterioration of the outermost enamel layer (Fig. 2, F and H). Histological analysis confirmed this observation, showing the absence of iron pigmentation in mutant incisors (Fig. 2, K to P).

To investigate the molecular mechanisms that underlie the enamel phenotype in the K14-Bcl9/9l-flox animals, we sought to understand whether Bcl9/9l exerted their roles in enamel formation by interacting with their known partners, β-catenin and Pygo2 (*2*, *4*, *5*, *7*). Therefore, we first abrogated the interaction between β-catenin and Bcl9/9l, which is mediated by the HD2 domains of Bcl9 and Bcl9l, by generating a genetic *Bcl9/9l* model in which these domains are deleted (K14-Cre; $Bcl9^{flox/\Delta HD2}$ $Bcl9l^{flox/\Delta HD2}$, abbreviated as K14-Bcl9/9l-ΔHD2; Fig. 3A) (*10*). Teeth of K14-Bcl9/9l-ΔHD2 mice did not display any obvious enamel defect and were indistinguishable from those of control littermates (Fig. 3, B to D). This demonstrates that Bcl9/9l function independently of β-catenin in enamel formation. We next investigated the effect of the other Bcl9/9l interactor, Pygo2, on amelogenesis. Although *Pygo1*-null mice have no distinguishable phenotype (*8*–*10*, *17*), to prevent any potential redundant role of Pygo1, we induced the simultaneous recombination of both *Pygo1* and *Pygo2*. The K14-Cre–mediated deletion of *Pygo1* and *Pygo2* (K14-Cre; $Pygo1^{flox/flox}$; $Pygo2^{flox/flox}$, abbreviated as K14-Pygo1/2-flox; Fig. 3E) recapitulated the enamel defects observed in the K14-Bcl9/9l-flox mice (Fig. 3, F to H). Notably, abrogating just the interaction between Bcl9/9l and Pygo1/2 proteins by removing the HD1 domains of Bcl9 and Bcl9l, in K14-Cre; $Bcl9^{flox/\Delta HD1}$; $Bcl9l^{flox/\Delta HD1}$ (K14-Bcl9/9l-ΔHD1) mice (*17*), was also sufficient to perturb enamel structure (fig. S4).

Cytoplasmic Bcl9 interacts with ameloblast-specific proteins

The observation that Bcl9/9l affected enamel formation independently of β-catenin–mediated gene transcription, together with the prominent cytoplasmic localization of Bcl9/9l, strongly suggested that Bcl9/9l may interact with molecules localized in the cytoplasm of ameloblasts. To test this, we collected ameloblasts from the incisors of newborn mice, extracted total protein, immunoprecipitated proteins that interacted with Bcl9, and analyzed these proteins by mass spectrometry (MS) (Fig. 4A and fig. S5). The ameloblast-specific Bcl9 interactome was significantly enriched for proteins associated with exocytosis, membrane-bound vesicles, and extracellular vesicular trafficking (Fig. 4B and table S1). This set of proteins included amelogenin, the main extracellular matrix protein required for enamel development and maturation (Fig. 4, B and C) (*18*, *19*). Consistent with the Bcl9/9l phenotype, amelogenin is required for the inclusion of minerals into the growing hydroxyapatite crystals that are the main component of enamel and, furthermore, for directing the organization of the enamel rods (*20*). Confocal immunofluorescence was performed to further analyze the possible interaction between amelogenin and Bcl9, and revealed that amelogenin and Bcl9 colocalized in the cytoplasm of secretory, mature ameloblasts (Fig. 4, D and E), consistent with the association of amelogenin and Bcl9 in these cells. We performed immunolabeling in incisors from K14-Bcl9/9l-flox mice and found that although amelogenin was still present, the pattern of its localization changed. Amelogenin appeared to be less abundant and present in smaller aggregations (Fig. 4F), suggesting a potential role of Bcl9/9l in amelogenin trafficking and secretion. We confirmed the decreased amount of amelogenin in incisors from K14-Bcl9/9l-flox mice by Western blot analysis (Fig. 4G). The abundance of *Amelx*, the transcript encoding amelogenin, was unaffected (Fig. 4H). Consistently, the abundances of mRNAs encoding other proteins known to be required for enamel formation were also unchanged in the mutants (Fig. 4H). We interpret these data as an additional indication that Bcl9/9l do not regulate enamel formation by influencing the rate of transcription of enamel-specific genes. Protein fractionation of ameloblasts confirmed that Bcl9 localized exclusively to the cytoplasm, whereas Pygo2 was found in both the cytoplasm and the nucleus of these cells (Fig. 4I). Bcl9 and Pygo2 appeared to colocalize only near the apical surface of ameloblasts (Fig. 4J), the same region where Bcl9 also colocalized with amelogenin, suggesting a potential role of the Bcl9-Pygo2 complex in the secretion of enamel components. The hypothesis that cytoplasmic Bcl9/9l act along

the secretory pathway is supported by confocal microscopy analysis showing that Bcl9/9l colocalize with calnexin and COP-I, which are markers of the endoplasmic reticulum and Golgi apparatus, respectively (figs. S6 and S7).

DISCUSSION

Here, we investigated the role of the Wnt/β-catenin transcriptional regulators Bcl9/9l and Pygo2 in the continuously growing mouse incisor, a model that allows the simultaneous investigation of processes involved in stem cell function and differentiation. Bcl9/9l and Pygo2 are both present in incisors, in the enamel-producing ameloblasts, where they are predominantly localized to the cytoplasm. The cytoplasmic localization was unexpected, given the role of these proteins as β-catenin transcriptional cofactors, and suggests that Bcl9/9l and Pygo1/2 have a nontranscriptional role in enamel formation.

Previous studies have shown that the loss of β-catenin in the dental epithelium causes tooth development to arrest at E14.5 in mice (*11*).

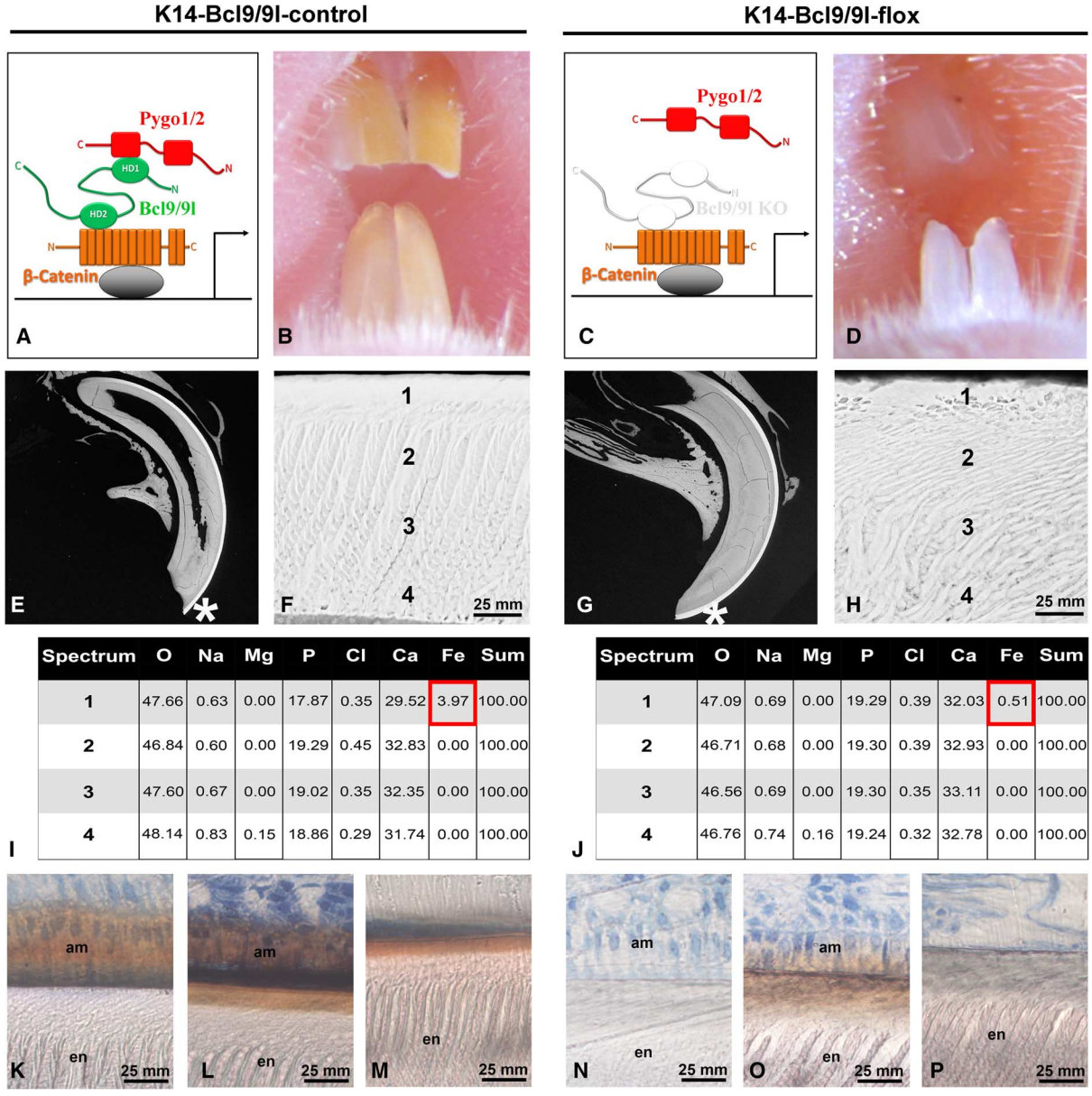

I	Spectrum	O	Na	Mg	P	Cl	Ca	Fe	Sum
	1	47.66	0.63	0.00	17.87	0.35	29.52	3.97	100.00
	2	46.84	0.60	0.00	19.29	0.45	32.83	0.00	100.00
	3	47.60	0.67	0.00	19.02	0.35	32.35	0.00	100.00
	4	48.14	0.83	0.15	18.86	0.29	31.74	0.00	100.00

J	Spectrum	O	Na	Mg	P	Cl	Ca	Fe	Sum
	1	47.09	0.69	0.00	19.29	0.39	32.03	0.51	100.00
	2	46.71	0.68	0.00	19.30	0.39	32.93	0.00	100.00
	3	46.56	0.69	0.00	19.30	0.35	33.11	0.00	100.00
	4	46.76	0.74	0.16	19.24	0.32	32.78	0.00	100.00

Fig. 2. Conditional loss of Bcl9/9l causes enamel defects in adult mice. (**A**) Bcl9/9l tether Pygo1/2 at the β-catenin transcriptional complex. (**B**) Adult incisors from control mice are yellow and opaque. (**C**) Disruption of the β-catenin transcriptional complex in K14-Bcl9/9l-flox mice. KO, knockout. (**D**) Incisors from K14-Bcl9/9l-flox mice are white and glassy. Note that both upper incisors are present in this animal, but one is fractured. (**E** to **H**) SEM imaging of incisors from wild-type (E and F) and mutant (G and H) mice. High-magnification views of the enamel (en) from the tooth tip [asterisks in (E) and (G)] reveal disruption of the highly ordered deposition of the hydroxyapatite rods in the Bcl9/9l mutant enamel (F and H). (**I** and **J**) EDS shows the relative elemental composition of enamel from the incisors of K14-Bcl9/9l and K14-Bcl9/9l-flox mice. The numbers in the left columns indicate the enamel regions analyzed at the tooth tip [asterisks in (E) and (G)]. (**K** to **P**) Toluidine staining of incisor sections from wild-type (K to M) and Bcl9/9l mutant (N to P) mice. For each set of images, the left image shows immature enamel from the base of the tooth (K and N), more mature enamel from the middle of the tooth (L and O), and fully maturated enamel from the tip of the tooth (M and P). $n > 3$ individual animals for each experiment.

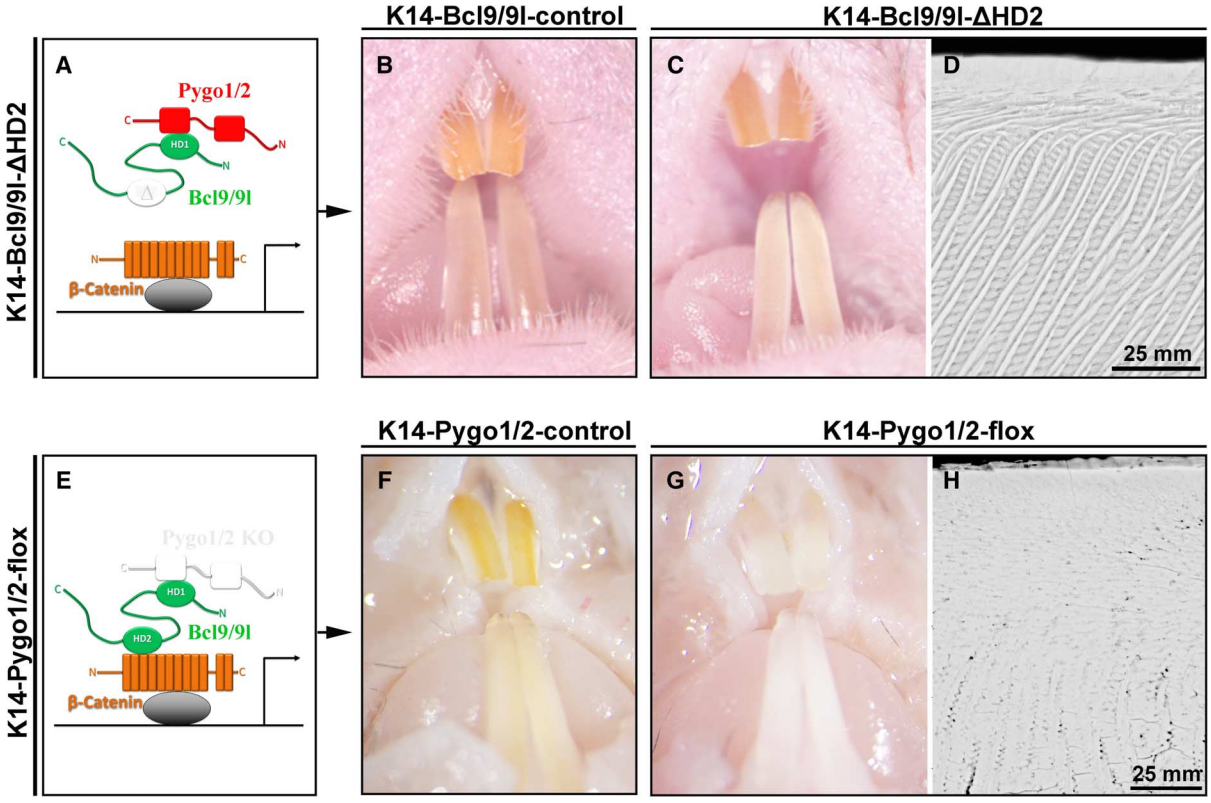

Fig. 3. β-Catenin transcription-independent, but Pygo-dependent, role of Bcl9/9l. (**A**) Deletion of the HD2 domain of Bcl9/9l prevents the Bcl9/9l-Pygo complex from interacting with β-catenin but does not affect the appearance of tooth enamel (**B** and **C**) or the ultrastructure of the enamel (**D**). (**E**) K14-Cre–mediated deletion of *Pygo1/2* in the oral epithelium affects the pigmentation of the tooth enamel (**F** and **G**) and the ultrastructure of the enamel (**H**) similarly to the loss of Bcl9/9l. $n > 3$ individual animals for each experiment.

However, β-catenin is a dual-function protein that both coordinates cell-cell adhesion at adherens junctions and promotes the expression of Wnt-dependent target genes (*2*). Consequently, deletion of β-catenin does not allow the contribution of these two distinct roles to be distinguished. We therefore exploited a mutation that produces a form of β-catenin that retains its function at the adherens junction but is unable to act as a transcriptional cofactor (*3*). We show that the loss of Wnt/β-catenin–dependent transcription recapitulates the complete deletion of β-catenin, thus conclusively demonstrating that the main role of β-catenin at the onset of odontogenesis is to mediate transcription that is dependent on canonical Wnt signaling.

Bcl9/9l and Pygo2 are important β-catenin transcriptional cofactors. In contrast to what we observed upon loss of β-catenin–dependent transcription, teeth develop in mice lacking Bcl9/9l in the dental epithelium. However, incisors of adult mutant mice displayed severe defects in enamel, such as disorganized hydroxyapatite enamel rods, which in wild-type teeth are arranged in tightly ordered three-dimensional arrays interspersed with interrod enamel. This peculiar arrangement of rods serves to deflect and arrest cracks within enamel, thus ensuring its hardness and resistance to mechanical stresses (*21*). Enamel is the most highly mineralized tissue in the mammalian body. It is mainly composed of minerals (97%), water, residual organic molecules, and small amounts of substituting ions that strongly affect its properties (*21*). In rodent incisors in particular, iron (Fe^{2+}) deposition is linked to the yellow pigmentation of the outermost layer of enamel and greatly increases its hardness (*16*). Moreover, iron provides additional resistance to bacterial toxins and acids, thus inhibiting pathological tooth alterations such as caries (*16*). Bcl9/9l mutant enamel is characterized by the nearly complete absence of iron. The combination of structural disorganization and iron deficiency in the enamel of *Bcl9/9l* mutant mice leads to a severe reduction of its resistance, which can lead to incisor fractures. We interpret this as an important evidence of the decreased enamel hardness in K14-Bcl9/9l-flox mice.

The function of Bcl9/9l in enamel formation is independent of their interaction with β-catenin, as shown by deletion of the Bcl9/9l HD2 domain, which mediates the interaction between β-catenin and Bcl9/9l (*10*). In contrast, *Pygo1/2* deletion recapitulated the enamel defects observed in the Bcl9/9l mutant mice, indicating that Pygo1/2 are important partners of Bcl9/9l in enamel formation. Abrogating the interaction between Bcl9/9l and Pygo1/2 was sufficient to induce defective enamel formation. We thus conclude that Bcl9/9l and Pygo1/2 act together as a functional unit to ensure proper amelogenesis, independently of β-catenin–dependent transcription. Collectively, our data indicate that Bcl9/9l and Pygo1/2 have fundamental roles in late tooth developmental processes such as enamel formation and maturation, in contrast with the early effects of β-catenin in odontogenesis.

The independence of Bcl9/9l from β-catenin–mediated transcription, together with their cytoplasmic localization in ameloblasts, prompted us to test whether Bcl9/9l interact with other cytoplasmic molecules to exert their specific functions. We found that Bcl9 associates with several proteins involved in exocytosis, membrane-bound vesicles, and trafficking of secretory vesicles. Surprisingly, amelogenin, which is the main extracellular matrix protein required for enamel development and maturation (*18*, *19*), was among the Bcl9 cytoplasmic interactors that we

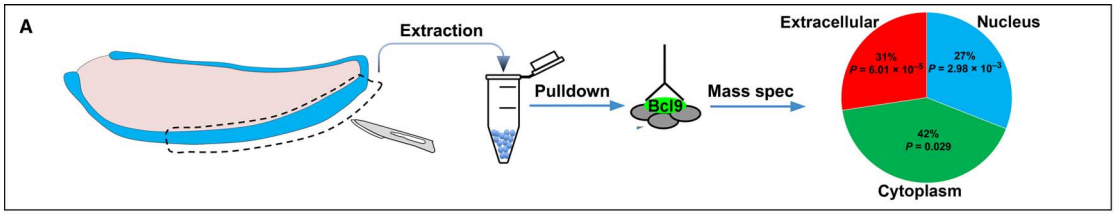

B

GO terms	FOLD ENRICHMENT	*P* VALUE	Examples
Extracellular exosome	4.25	6.98×10^{-7}	Annexin A1, Annexin A6 Lumican
Extracellular vesicle	4.23	7.69×10^{-7}	
Extracellular organelle	4.22	8.05×10^{-7}	
Membrane-bounded vesicle	3.5	2.68×10^{-5}	
Vesicle	3.22	1.23×10^{-4}	
Extracellular region part	3.21	5.64×10^{-5}	Amelogenin X

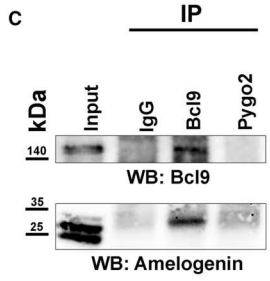

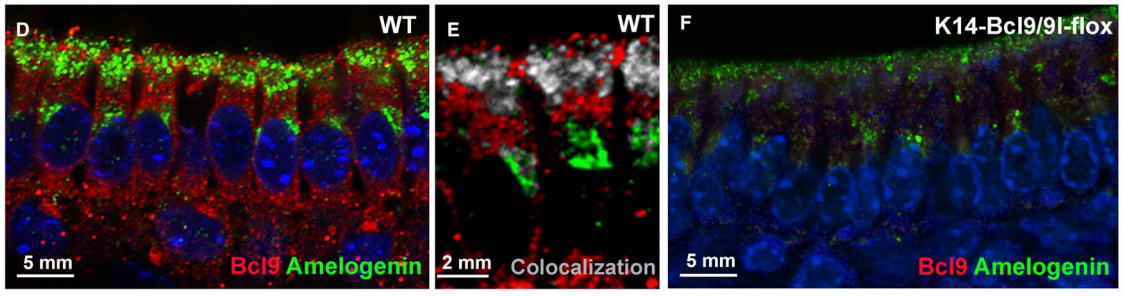

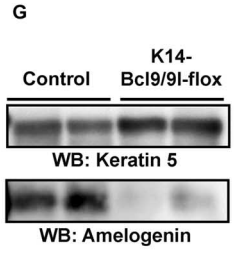

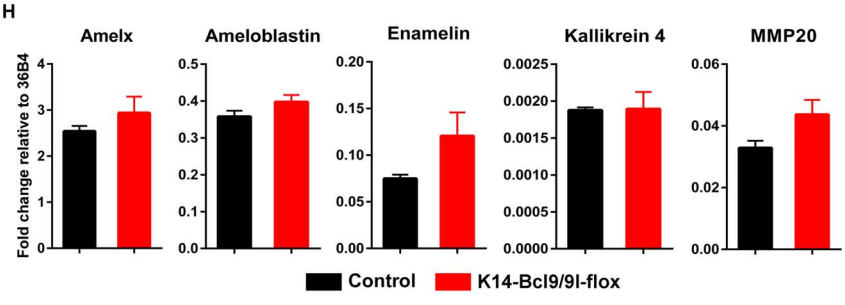

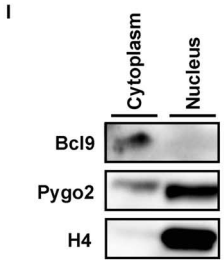

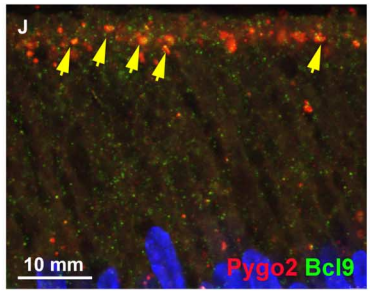

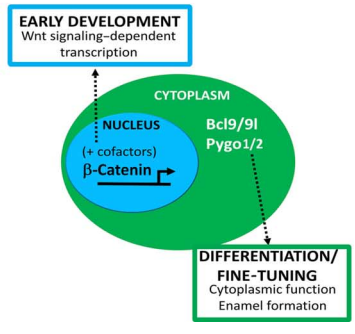

Fig. 4. Bcl9 interactome in the ameloblasts. (**A**) Workflow for ameloblast dissection and Bcl9 interactome analysis. $n = 2$. (**B**) The ameloblast-specific Bcl9 interactome is enriched with proteins involved in protein trafficking and secretion. GO, Gene Ontology. (**C**) Western blot (WB) validation of the interaction between Bcl9 and amelogenin in Bcl9 immunoprecipitates (IP) of ameloblast extracts from wild-type (WT) mice. $n = 2$. IgG, immunoglobulin G. (**D**) Representative confocal immunofluorescence analysis of Bcl9 and amelogenin in ameloblasts. $n = 3$ different mice. (**E**) Colocalization of Bcl9 and amelogenin in ameloblasts. Gray indicates the areas of colocalization on a single focal plane. (**F**) Amelogenin localization in ameloblasts from K14-Bcl9/9l-flox mice. (**G**) Western blot for amelogenin in protein extracts from ameloblasts of K14-Bcl9/9l-control (Control) and K14-Bcl9/9l-flox mice. Keratin 5 was used as a loading control. Each lane represents an independent individual mouse; $n = 2$ for each genotype. (**H**) Quantitative real-time polymerase chain reaction (qRT-PCR) to quantify the abundance of transcripts important for enamel formation in isolated dental epithelia from K14-Bcl9/9l-control mice (black bars) and K14-Bcl9/9l-flox mice (red bars). $n = 5$. (**I**) Western blot showing Bcl9 and Pygo2 in cytoplasmic and nuclear fractions of protein extracts from ameloblasts. $n = 2$. Histone H4 was used to specifically mark the nuclear fraction. (**J**) Representative confocal microscopy image showing localization of Bcl9 (green) and Pygo2 (red) in wild-type ameloblasts. $n = 2$. The signals overlap at the most apical secretory region of ameloblasts (arrows). (**K**) Whereas β-catenin–dependent gene transcription is important for early tooth development, Bcl9/9l and Pygo1/2 function in the cytoplasm as key determinants of late enamel development.

detected. The importance of this molecule in enamel formation has been highlighted in human pathologies affecting teeth, where mutations in *AMELX*, the gene encoding amelogenin, cause severe enamel defects collectively referred to as amelogenesis imperfecta (*22*). Notably, the enamel phenotype observed upon mutation of *Bcl9/9l* closely resembles that previously observed in mice harboring a mutation in the N terminus

of amelogenin (*23*, *24*). We speculate that the proper function of amelogenin requires its interaction with Bcl9/9l, and perhaps this interaction is mediated by the N-terminal domain of amelogenin. In the incisors of *Bcl9/9l* mutant mice, both amelogenin localization and abundance appear impaired when compared to control specimens. Nevertheless, the deletion of *Bcl9/9l* does not lead to significant alterations in the expression of the genes encoding amelogenin or other proteins important for enamel formation, such as ameloblastin, enamelin, kallikrein 4, and MMP20. This is consistent with a nontranscriptional role of Bcl9/9l in amelogenesis, which is further supported by (i) the absence of Bcl9 in the nucleus, (ii) the colocalization of Bcl9/9l with Pygo2 at the apical secretory domain of ameloblasts, and (iii) the colocalization of Bcl9/9l with molecules specific for the Golgi apparatus and endoplasmic reticulum. Although we cannot exclude that Bcl9 and Pygo2 may still retain some nuclear function in this context, we show that they do not participate in β-catenin–dependent transcription during early odontogenesis. At later developmental stages, the Bcl9-Pygo2 complex fine-tunes enamel formation by direct physical interaction with ameloblast-specific proteins without regulating their transcription. It should be interesting to investigate the role of Bcl9/9l and Pygo1/2 in other cell types that produce mineralized extracellular matrices, such as the odontoblasts and osteoblasts.

The requirement for Bcl9/9l and Pygo1/2 in many contexts has been attributed to these proteins acting as transcriptional regulators of Wnt signaling (*2*, *25*, *26*). Our work provides the alternative explanation that Bcl9/9l and Pygo1/2 can act in the cytoplasm, independently of β-catenin, and are key determinants that can regulate developmental processes. Thus, these transcriptional regulators of the highly conserved Wnt signaling pathway can fine-tune late developmental events through a previously undetected cytoplasmic activity (Fig. 4K). We propose that Bcl9/9l and Pygo1/2 might exert this function by influencing the trafficking or the stability of enamel-building proteins and iron deposition through an as yet unidentified mechanism. This new role could represent an example of exaptation, the co-option of these proteins during the evolution of enamel, a highly specialized material present only in vertebrates (*27*, *28*). On the other hand, these functions might constitute more general features of Bcl9/9l and Pygo1/2 that have so far been completely overlooked.

Despite their clinical relevance, the molecular mechanisms responsible for the observed variability in tooth properties in humans are essentially unknown. The finely tuned structure of enamel is of crucial importance for its ability to resist insults, such as bacterial toxins, acids, and mechanical stresses that can lead to various dental pathologies. Bcl9/9l and Pygo1/2 are fundamental to maintaining the structural integrity of enamel. It is tantalizing to hypothesize that genetic variations or mutations in the genes encoding these proteins might influence the predisposition to dental defects related to enamel fragility in humans. Thus, as hitherto unrecognized players in the fine-tuning of the enamel structure and composition, Bcl9/9l and Pygo1/2 may contribute to the differential susceptibility to dental pathologies in humans.

MATERIALS AND METHODS

Animals and tissue processing

All mice were maintained and handled according to the Swiss Animal Welfare Law and in compliance with the regulations of the Cantonal Veterinary Office, Zurich. The mutant animals used in this study were generated by crossing mutant alleles in *Ctnnb1*, *Bcl9/9l*, and *Pygo1/2* with a *K14-Cre* recombinase driver. For the generation of the conditional *Bcl9/9l* alleles, see the study by Deka *et al.* (*15*); for the generation of the *Pygo1/2* conditional alleles, see the study by Cantù *et al.* (*17*). The *Bcl9/9l* deletion mutants were generated by Cantù *et al.* (*10*). The β-*catenin* dm allele (transcriptionally null, "double mutant") was generated by Valenta *et al.* (*3*). To facilitate the complete recombination of the alleles, we generated "K14-Bcl9/9l-flox" mice by crossing the LoxP-containing alleles (K14-Cre; $Bcl9^{flox/flox}$ $Bcl9^{flox/flox}$) with constitutive null alleles ($Bcl9^{flox/KO}$ $Bcl9l^{flox/KO}$) in K14-Cre; $Bcl9^{flox/KO}$; $Bcl9l^{flox/KO}$ mice.

Embryonic age was determined according to the vaginal plug (day 0) and confirmed by morphological criteria. Pregnant animals were sacrificed by cervical dislocation, and the embryos were surgically removed into Dulbecco's phosphate-buffered saline (PBS; pH 7.4). Dissected heads from the E14.5 and P0 pups were fixed in 4% paraformaldehyde (PFA) in PBS for 24 hours at 4°C.

Adult animals were anesthetized with ketamine/xylazine and perfused with 4% PFA. Heads were then postfixed for up to 7 days in 4% PFA. For immunohistochemical analysis, fixed heads were then decalcified in 10% EDTA, dehydrated, and embedded in paraffin.

Immunohistochemistry

Immunohistochemistry was performed on 5- to 10-μm-thick paraffin sections. Briefly, endogenous peroxidases were quenched in a solution of 0.3% H_2O_2 in methanol, and heat-induced antigen retrieval in 10 mM trisodium citrate buffer (pH 6.0) was performed. For the staining procedure, the Vectastain ABC Kit was used (ABC Kit, Vector Laboratories). As a chromogenic substrate, SIGMA*FAST* 3,3′-Diaminobenzidine tablets (D4293, Sigma-Aldrich) were used. Omission of the primary antibody served as a negative control. Stained sections were counterstained with toluidine blue and mounted with Glycergel (C0563, Dako North America Inc.). Pictures were taken using the Leica DFC420C camera and the Leica Application Suite (LAS) software. The following primary antibodies were used: anti-BCL9 (ab54833 or ab37305, Abcam), anti-BCL9l (PAB19408, Abnova), anti-Pygo2 (NBP1-46171, Novus Biologicals), anti–β-catenin (clone 14, 610154, BD), anti–amelogenin X (ab153915, Abcam), anti–COP-I (ab6323, Abcam), and anti-calnexin (ab31290, Abcam).

Immunofluorescence

Immunofluorescence was performed on 5- to 10-μm-thick paraffin sections. Heat-induced antigen retrieval in 10 mM trisodium citrate buffer (pH 6.0) was performed, followed by blocking in a solution of PBS + 2% normal goat/donkey serum + 0.5% Tween 20. The sections were then incubated with primary antibodies (see above) dissolved in blocking solution overnight at 4°C. After extensive washing with PBS, the sections were then incubated with a fluorescently labeled secondary antibody (Alexa 488 goat anti-mouse and Alexa 555 goat anti-rabbit, 1:500). Nuclei were stained with 4′,6-diamidino-2-phenylindole (1:1000, Sigma-Aldrich Chemie). Slides were mounted with FluorSave Reagent (345789, Merck Millipore) and imaged with a Zeiss LSM 710 confocal microscope, using a pinhole size of 1 airy unit to capture emission wavelength deriving from a single focal plane.

Western blot

Total protein extracts were prepared according to standard protocols. Cytoplasmic versus nuclear protein fractionation was performed as previously described (*17*), and proteins were subjected to SDS–polyacrylamide gel electrophoresis (SDS-PAGE) separation and blotting. The following antibodies were used: anti-Pygo2 (NBP1-46171, Novus Biological; sc-74878,

Santa Cruz Biotechnology), anti-BCL9 (ab54833 or ab37305, Abcam), anti–histone H4 (Upstate), anti–keratin 5 (PRB-160P, BioLegend), and anti–amelogenin X (ab153915, Abcam). Antibody binding was detected by using an appropriate horseradish peroxidase–conjugated IgG and revealed by ECL (GE Healthcare).

Microcomputed tomography

Adult perfused mouse heads were washed in PBS and progressively dehydrated to 70% ethanol for microcomputed tomography (μCT) analysis. The μCT scans were performed using a commercially available μCT unit (Specimen μCT 40, Scanco Medical), with all imaging parameters kept identical during all examinations (tube voltage, 70 kV; tube current, 114 μA; isotropic resolution, 18 μm). The original images were converted into the RAW format using the proprietary software of the μCT device and imported in the three-dimensional reconstruction program VGStudio MAX (Volume Graphics). All the analyzed samples were segmented manually using wild-type teeth as reference for the gray-level values corresponding to the single mineralized tissues (enamel, dentin, and bone).

Backscattered SEM and elemental analysis

Fully mineralized lower hemijaws were dissected from perfused adult (about 3 months of age) K14-Bcl9/9l-flox, K14-Bcl9/9l-ΔHD2, and K14-Pygo1/2-flox and the respective Bcl9/9l-flox, Bcl9/9l-ΔHD2, and Pygo1/2-flox controls. Soft tissues were removed manually. The lower jaws were then dehydrated and embedded in Technovit 7200 VLC (Heraeus Kulzer). Light-polymerized blocks were mounted on aluminum stubs, polished, and coated with a 10- to 15-nm-thick layer of carbon. Thereafter, they were examined using a Tescan EGATS5316 XMSEM operated in backscattered electron mode. Elemental composition of enamel was analyzed with the aid of EDS. A Si(Li) detector (Oxford Instruments) served for recording EDS spectra using an accelerating voltage of 7 kV, a working distance of 23 mm, and a counting time of 100 s. For the quantitative analysis of these spectra, the INCA energy software (Oxford Instruments) was used.

Immunoprecipitation and MS

Dissected ameloblasts were minced in cold PBS and treated with a hypotonic lysis buffer (20 mM tris-HCl, 75 mM NaCl, 1.5 mM $MgCl_2$, 1 mM EGTA, 0.5% NP-40, and 5% glycerol). Protein extracts obtained were incubated with 1 μg of anti-BCL9 antibody (ab54833 or ab37305, Abcam) and protein A–conjugated Sepharose beads (GE Healthcare); they were then diluted in lysis buffer to a final volume of 1 ml. After 4 hours of incubation at 4°C on a rotating wheel, the beads were spun down and washed three times in lysis buffer. All steps were performed on ice, and all buffers were supplemented with fresh protease inhibitors (cOmplete, Roche) and 1 mM phenylmethylsulfonyl fluoride. For detecting the proteins in Western blot, the pulldown reactions were treated with Laemmli buffer, boiled at 95°C for 15 min, and subjected to SDS-PAGE separation and blotting on a polyvinylidene difluoride (PVDF) membrane. The PVDF membrane was probed with the anti–amelogenin X.

For liquid chromatography–MS/MS analysis, the protein samples, already dissolved in Laemmli buffer, were submitted to a filter-aided sample preparation (FASP) as described in (*29*) and digested with trypsin in 100 mM triethylammonium bicarbonate buffer overnight. Desalted samples were dried completely in a vacuum centrifuge and reconstituted with 50 μl of 3% acetonitrile and 0.1% formic acid. Each peptide solution (4 μl) was analyzed on both Q Exactive and Fusion mass spectrometers (Thermo Scientific) coupled to EASY-nLC 1000 (Thermo Scientific). On the Q Exactive, full-scan MS spectra were acquired in profile mode from 300 to 1700 mass/charge ratio (*m/z*) with an automatic gain control target of 3×10^6, an Orbitrap resolution of 70,000 (at 200 *m/z*), and a maximum injection time of 120 ms. The 12 most intense multiply charged (z = +2 to +8) precursor ions from each full scan were selected for higher-energy collisional dissociation fragmentation with a normalized collision energy of 30 arbitrary unit. Generated fragment ions were scanned with an Orbitrap resolution of 35,000 (at 200 *m/z*), an automatic gain control value of 5×10^4, and a maximum injection time of 120 ms. The isolation window for precursor ions was set to 2.0 *m/z*, and the underfill ratio was at 1% (referring to an intensity of 4.2×10^3). Each fragmented precursor ion was set onto the dynamic exclusion list for 90 s. For the Orbitrap Fusion, the "Universal Method" as described in (*30*) was applied. Peptide separation on both instruments was achieved by reversed-phase high-performance liquid chromatography on an in-house packed C18 column (150 mm × 75 μm, 1.9 μm, C-18 AQ, 120 Å; Dr. Maisch GmbH). Samples were loaded with maximum speed at a pressure restriction of 400 bar and separated with a linear gradient from 3 to 25% solvent B (0.1% formic acid in acetonitrile, Biosolve BV) in solvent A (0.1% formic acid in H_2O, Biosolve BV) at a flow rate of 250 nl/min. The column was washed after the separation by flushing with 95% solvent B for 10 min, automatically equilibrated before the next injection, and exported to mgf (Mascot generic format) format for subsequent database search.

Peak lists were extracted from the instrument raw files using ProteomeDiscoverer (version 1.4) in combination with the FCC [FGCZ (Functional Genomics Center Zurich) Converter Control] (*31*) and exported to mgf format for subsequent database search. All MS/MS samples were analyzed using Mascot (Matrix Science, version 2.4.1). Mascot was set up to search the fgcz_10090_20140715 database (http://fgcz-s-021.uzh.ch/fasta/fgcz_10090_20140715.fasta, 51,806 entries), assuming the digestion enzyme trypsin, and the fgcz_10090_d_20140715 database (http://fgcz-s-021.uzh.ch/fasta/fgcz_10090_d_20140715.fasta, 103,351 entries), also assuming trypsin. Mascot was searched with a fragment ion mass tolerance of 0.050 Da and a parent ion tolerance of 10.0 parts per million. Carbamidomethyl of cysteine was specified in Mascot as a fixed modification. Oxidation of methionine was specified in Mascot as a variable modification. Scaffold (version Scaffold_4.4.1, Proteome Software Inc.) was used to validate MS/MS-based peptide and protein identifications. Peptide identifications were accepted if they could be established at greater than 95% probability by the PeptideProphet algorithm (*32*) with Scaffold delta-mass correction. Protein identifications were accepted if they could be established at greater than 95.0% probability and contained at least two identified peptides. Protein probabilities were assigned by the ProteinProphet algorithm (*33*). Proteins that contained similar peptides and could not be differentiated on the basis of MS/MS analysis alone were grouped to satisfy the principles of parsimony. Proteins sharing significant peptide evidence were grouped into clusters. DAVID (Database for Annotation, Visualization and Integrated Discovery) software (version DAVID 6.7, http://david.ncifcrf.gov) was used to determine whether a gene product is located in or is a subcomponent of a particular cellular component. The MS data have been deposited in the PRIDE (Proteomics Identifications) Archive database (*34*) with the data set identifier PXD005449.

RNA isolation and qRT-PCR

Total RNA was isolated from incisors dissected from pups using the RNeasy Plus Universal Mini Kit (Qiagen) and further purified by ethanol precipitation. RNA retrotranscription was performed using the iScript

Reverse Transcription Kit (Bio-Rad). qRT-PCR was performed in the Illumina Eco Real-Time PCR System (Illumina), using Power SYBR Green (Life Technologies) as reaction mix. The following primers were used: amelogenin X (5′-CCCTACCACCTCATCCTGGA-3′, 5′-GAGGCTGAAGGGTGTGACTC-3′), ameloblastin (5′-AGTGAAAA-TGAGCCTCGCCG-3′, 5′-CGTTGAGTCCCTGCAAGCTT-3′), enamelin (5′-GTCTCTGCTGCCATGCCATT-3′, 5′-GGAGGGTACTGTGGAGG-CAT-3′), kallikrein 4 (5′-TTGCAAACGATCTCATGCTC-3′, 5′-TGA-GGTGGTACACAGGGTCA-3′), and MMP20 (5′-CTTTCCCCAGCT-AATGTCCA-3′, 5′-CTTGGGAACCCGAAGTCATA-3′). For a comparison of the groups, a multiple *t* test analysis was performed using GraphPad Prism version 6.05 (GraphPad Software Inc.). Data were considered significant at $P < 0.05$.

SUPPLEMENTARY MATERIALS

www.sciencesignaling.org/cgi/content/full/10/465/eaah4598/DC1

Fig. S1. Bcl9 and Pygo2 are present in differentiated, secretory ameloblasts but not in the stem cell niche.

Fig. S2. β-Catenin transcriptional output is required for early tooth development.

Fig. S3. K14-Cre–mediated deletion of *Bcl9/9l* does not cause early tooth development arrest.

Fig. S4. The Bcl9/9l-Pygo1/2 interaction is required for proper enamel formation.

Fig. S5. Ameloblast-specific Bcl9 interactors.

Fig. S6. Bcl9 and Bcl9l are present in the cytoplasm along the secretory pathway.

Fig. S7. Bcl9 and Bcl9l colocalize with the secretory pathway proteins calnexin and COP-I.

Table S1. Proteins found in two independent pulldown experiments using an antibody recognizing Bcl9 and subtracting the proteins retrieved by pulldown with control preimmune IgG.

REFERENCES AND NOTES

1. H. Clevers, Wnt/β-catenin signaling in development and disease. *Cell* **127**, 469–480 (2006).
2. C. Mosimann, G. Hausmann, K. Basler, β-Catenin hits chromatin: Regulation of Wnt target gene activation. *Nat. Rev. Mol. Cell Biol.* **10**, 276–286 (2009).
3. T. Valenta, M. Gay, S. Steiner, K. Draganova, M. Zemke, R. Hoffmans, P. Cinelli, M. Aguet, L. Sommer, K. Basler, Probing transcription-specific outputs of β-catenin in vivo. *Genes Dev.* **25**, 2631–2643 (2011).
4. T. Kramps, O. Peter, E. Brunner, D. Nellen, B. Froesch, S. Chatterjee, M. Murone, S. Züllig, K. Basler, Wnt/Wingless signaling requires BCL9/legless-mediated recruitment of pygopus to the nuclear β-catenin-TCF complex. *Cell* **109**, 47–60 (2002).
5. B. Thompson, F. Townsley, R. Rosin-Arbesfeld, H. Musisi, M. Bienz, A new nuclear component of the Wnt signalling pathway. *Nat. Cell Biol.* **4**, 367–373 (2002).
6. R. Städeli, K. Basler, Dissecting nuclear Wingless signalling: Recruitment of the transcriptional co-activator Pygopus by a chain of adaptor proteins. *Mech. Dev.* **122**, 1171–1182 (2005).
7. R. Hoffmans, R. Städeli, K. Basler, Pygopus and legless provide essential transcriptional coactivator functions to Armadillo/β-catenin. *Curr. Biol.* **15**, 1207–1211 (2005).
8. K. R. Schwab, L. T. Patterson, H. A. Hartman, N. Song, R. A. Lang, X. Lin, S. S. Potter, *Pygo1* and *Pygo2* roles in Wnt signaling in mammalian kidney development. *BMC Biol.* **5**, 15 (2007).
9. B. Li, C. Rhéaume, A. Teng, V. Bilanchone, J. E. Munguia, M. Hu, S. Jessen, S. Piccolo, M. L. Waterman, X. Dai, Developmental phenotypes and reduced wnt signaling in mice deficient for *pygopus* 2. *Genesis* **45**, 318–325 (2007).
10. C. Cantù, D. Zimmerli, G. Hausmann, T. Valenta, A. Moor, M. Aguet, K. Basler, Pax6-dependent, but β-catenin-independent, function of Bcl9 proteins in mouse lens development. *Genes Dev.* **28**, 1879–1884 (2014).
11. F. Liu, E. Y. Chu, B. Watt, Y. Zhang, N. M. Gallant, T. Andl, S. H. Yang, M.-M. Lu, S. Piccolo, R. Schmidt-Ullrich, M. M. Taketo, E. E. Morrisey, R. Atit, A. A Dlugosz, S. E. Millar, Wnt/β-catenin signaling directs multiple stages of tooth morphogenesis. *Dev. Biol.* **313**, 210–224 (2008).
12. E. Järvinen, I. Salazar-Ciudad, W. Birchmeier, M. M. Taketo, J. Jernvall, I. Thesleff, Continuous tooth generation in mouse is induced by activated epithelial Wnt/β-catenin signaling. *Proc. Natl. Acad. Sci. U.S.A.* **103**, 18627–18632 (2006).
13. Z. Yang, A. Balic, F. Michon, E. Juuri, I. Thesleff, Mesenchymal Wnt/β-catenin signaling controls epithelial stem cell homeostasis in teeth by inhibiting the antiapoptotic effect of Fgf10. *Stem Cells* **33**, 1670–1681 (2015).
14. T. A. Mitsiadis, D. Graf, Cell fate determination during tooth development and regeneration. *Birth Defects Res. C Embryo Today* **87**, 199–211 (2009).
15. J. Deka, N. Wiedemann, P. Anderle, F. Murphy-Seiler, J. Bultinck, S. Eyckerman, J.-C. Stehle, S. André, N. Vilain, O. Zilian, S. Robine, M. Delorenzi, K. Basler, M. Aguet, Bcl9/Bcl9l are critical for Wnt-mediated regulation of stem cell traits in colon epithelium and adenocarcinomas. *Cancer Res.* **70**, 6619–6628 (2010).
16. L. M. Gordon, M. J. Cohen, K. W. MacRenaris, J. D. Pasteris, T. Seda, D. Joester, Amorphous intergranular phases control the properties of rodent tooth enamel. *Science* **347**, 746–750 (2015).
17. C. Cantù, T. Valenta, G. Hausmann, N. Vilain, M. Aguet, K. Basler, The Pygo2-H3K4me2/3 interaction is dispensable for mouse development and Wnt signaling-dependent transcription. *Development* **140**, 2377–2386 (2013).
18. T. A. Mitsiadis, A. Filatova, G. Papaccio, M. Goldberg, I. About, P. Papagerakis, Distribution of the amelogenin protein in developing, injured and carious human teeth. *Front. Physiol.* **5**, 1 (2014).
19. M. K. Pugach, C. W. Gibson, Analysis of enamel development using murine model systems: Approaches and limitations. *Front. Physiol.* **5**, 313 (2014).
20. J. D. Bartlett, Dental enamel development: Proteinases and their enamel matrix substrates. *ISRN Dent.* **2013**, 684607 (2013).
21. A. Nanci, *Ten Cate's Oral Histology: Development, Structure, and Function* (Elsevier Inc., 2013).
22. J. T. Wright, The molecular etiologies and associated phenotypes of amelogenesis imperfecta. *Am. J. Med. Genet. A* **140**, 2547–2555 (2006).
23. C. W. Gibson, Z.-A Yuan, B. Hall, G. Longenecker, E. Chen, T. Thyagarajan, T. Sreenath, J. T. Wright, S. Decker, R. Piddington, G. Harrison, A. B. Kulkarni, Amelogenin-deficient mice display an amelogenesis imperfecta phenotype. *J. Biol. Chem.* **276**, 31871–31875 (2001).
24. M. J. Barron, S. J. Brookes, J. Kirkham, R. C. Shore, C. Hunt, A. Mironov, N. J. Kingswell, J. Maycock, C. A. Shuttleworth, M. J. Dixon, A mutation in the mouse Amelx tri-tyrosyl domain results in impaired secretion of amelogenin and phenocopies human X-linked amelogenesis imperfecta. *Hum. Mol. Genet.* **19**, 1230–1247 (2010).
25. A. E. Moor, P. Anderle, C. Cantù, P. Rodriguez, N. Wiedemann, F. Baruthio, J. Deka, S. André, T. Valenta, M. B. Moor, B. Győrffy, D. Barras, M. Delorenzi, K. Basler, M. Aguet, BCL9/9L-β-catenin signaling is associated with poor outcome in colorectal cancer. *EBioMedicine* **2**, 1932–1943 (2015).
26. K. Takada, D. Zhu, G. H. Bird, K. Sukhdeo, J.-J. Zhao, M. Mani, M. Lemieux, D. E. Carrasco, J. Ryan, D. Horst, M. Fulciniti, N. C. Munshi, W. Xu, A. L. Kung, R. A. Shivdasani, L. D. Walensky, D. R. Carrasco, Targeted disruption of the BCL9/β-catenin complex inhibits oncogenic Wnt signaling. *Sci. Transl. Med.* **4**, 148ra117 (2012).
27. S. Gould, E. Vrba, Exaptation—A missing term in the science of form. *Paleobiology* **8**, 4–15 (1982).
28. E. Renvoisé, F. Michon, An Evo-Devo perspective on ever-growing teeth in mammals and dental stem cell maintenance. *Front. Physiol.* **5**, 324 (2014).
29. J. R. Wiśniewski, A. Zougman, N. Nagaraj, M. Mann, Universal sample preparation method for proteome analysis. *Nat. Methods* **6**, 359–362 (2009).
30. G. Fascellaro, A. Petrera, Z. W. Lai, P. Nanni, J. Grossmann, S. Burger, M. L. Biniossek, A. Gomez-auli, O. Schilling, F. Imkamp, Comprehensive proteomic analysis of nitrogen-starved *Mycobacterium smegmatis* Δ*pup* reveals the impact of pupylation on nitrogen stress response. *J. Proteome Res.* **15**, 2812–2825 (2016).
31. S. Barkow-Oesterreicher, T. Can, C. Panse, FCC—An automated rule-based processing tool for life science data. *Source Code Biol. Med.* **8**, 3 (2013).
32. A. Keller, A. I. Nesvizhskii, E. Kolker, R. Aebersold, Empirical statistical model to estimate the accuracy of peptide identifications made by MS/MS and database search. *Anal. Chem.* **74**, 5383–5392 (2002).
33. A. I. Nesvizhskii, A. Keller, E. Kolker, R. Aebersold, A statistical model for identifying proteins by tandem mass spectrometry. *Anal. Chem.* **75**, 4646–4658 (2003).
34. J. A. Vizcaíno, A. Csordas, N. del-Toro, J. A. Dianes, J. Griss, I. Lavidas, G. Mayer, Y. Perez-Riverol, F. Reisinger, T. Ternent, Q.-W. Xu, R. Wang, H. Hermjakob, 2016 update of the PRIDE database and its related tools. *Nucleic Acids Res.* **44**, D447–D456 (2016).

Acknowledgments: We are much indebted to J. Hoffmann for assisting with the SEM analyses, E. Escher for technical help with mouse genotyping, and C. Trachsel and P. Nanni at the FGCZ for their supervision with MS experiments. **Funding:** This work was supported by the Swiss National Science Foundation (to K.B. and T.A.M.), grants from the Forschungskredit of the University of Zurich (to C.C.), by the University of Zurich (to P.P. and T.A.M.), and by the URPP (University Research Priority Programs) Translational Cancer Research Zurich (to T.V.). **Author contributions:** C.C. and P.P. designed the project, performed the

experiments, interpreted the data, and wrote the manuscript; T.D.S. assisted with immunofluorescence stainings; D.Z. and T.V. assisted with mouse breeding and genotyping; G.H. helped with the design of the work and critically revised the article; and K.B. and T.A.M. supervised and assisted the research team and provided ideas and critical revision of the manuscript. **Competing interests:** The authors declare that they have no competing interests. **Data and materials availability:** The MS proteomics data have been deposited to the ProteomeXchange Consortium via the PRIDE partner repository with the data set identifier PXD005449.

Submitted 29 June 2016
Accepted 4 January 2017
Published 7 February 2017
10.1126/scisignal.aah4598

Citation: C. Cantù, P. Pagella, T. D. Shajiei, D. Zimmerli, T. Valenta, G. Hausmann, K. Basler, T. A. Mitsiadis, A cytoplasmic role of Wnt/β-catenin transcriptional cofactors Bcl9, Bcl9l, and Pygopus in tooth enamel formation. *Sci. Signal.* **10**, eaah4598 (2017).

Science Signaling

A cytoplasmic role of Wnt/β-catenin transcriptional cofactors Bcl9, Bcl9l, and Pygopus in tooth enamel formation

Claudio Cantù, Pierfrancesco Pagella, Tania D. Shajiei, Dario Zimmerli, Tomas Valenta, George Hausmann, Konrad Basler and Thimios A. Mitsiadis

Sci. Signal. **10** (465), eaah4598.
DOI: 10.1126/scisignal.aah4598

Cytoplasmic functions for transcriptional cofactors in teeth

Bcl9, Bcl9l, and Pygo2 interact with transcription factors, such as the Wnt-regulated protein β-catenin, to regulate gene expression. Cantù *et al*. reveal that these proteins also have cytoplasmic functions during tooth development and are particularly important for the formation of enamel. Mice lacking both Pygo1 and Pygo2 or both Bcl9 and Bcl9l developed teeth, a process that requires Wnt/β-catenin transcriptional regulation, but the enamel was structurally disorganized and contained less iron than teeth from control mice. Bcl9, Bcl9l, and Pygo2 were present in the cytoplasm of ameloblasts, the cells that secrete enamel proteins, and colocalized in these cells with amelogenin, the main component of enamel. Bcl9 interacted with amelogenin and proteins involved in exocytosis and vesicular trafficking, suggesting that these proteins function in the trafficking or secretion of enamel proteins. These results demonstrate that Bcl9, Bcl9l, and Pygo2 have cytoplasmic functions distinct from their roles as transcriptional cofactors downstream of Wnt signaling.

Science Signaling
AAAS

www.sciencesignaling.org/cgi/content/full/10/465/eaah4598/DC1

Supplementary Materials for

A cytoplasmic role of Wnt/β-catenin transcriptional cofactors Bcl9, Bcl9l, and Pygopus in tooth enamel formation

Claudio Cantù, Pierfrancesco Pagella, Tania D. Shajiei, Dario Zimmerli, Tomas Valenta, George Hausmann, Konrad Basler,* Thimios A. Mitsiadis*

*Corresponding author. Email: konrad.basler@imls.uzh.ch (K.B.); thimios.mitsiadis@zzm.uzh.ch (T.A.M.)

Published 7 February 2017, *Sci. Signal.* **10**, eaah4598 (2017)
DOI: 10.1126/scisignal.aah4598

This PDF file includes:

Fig. S1. Bcl9 and Pygo2 are present in differentiated, secretory ameloblasts but not in the stem cell niche.
Fig. S2. β-Catenin transcriptional output is required for early tooth development.
Fig. S3. K14-Cre–mediated deletion of *Bcl9/9l* does not cause early tooth development arrest.
Fig. S4. The Bcl9/9l-Pygo1/2 interaction is required for proper enamel formation.
Fig. S5. Ameloblast-specific Bcl9 interactors.
Fig. S6. Bcl9 and Bcl9l are present in the cytoplasm along the secretory pathway.
Fig. S7. Bcl9 and Bcl9l colocalize with the secretory pathway proteins calnexin and COP-I.
Table S1. Proteins found in two independent pulldown experiments using an antibody recognizing Bcl9 and subtracting the proteins retrieved by pulldown with control preimmune IgG.

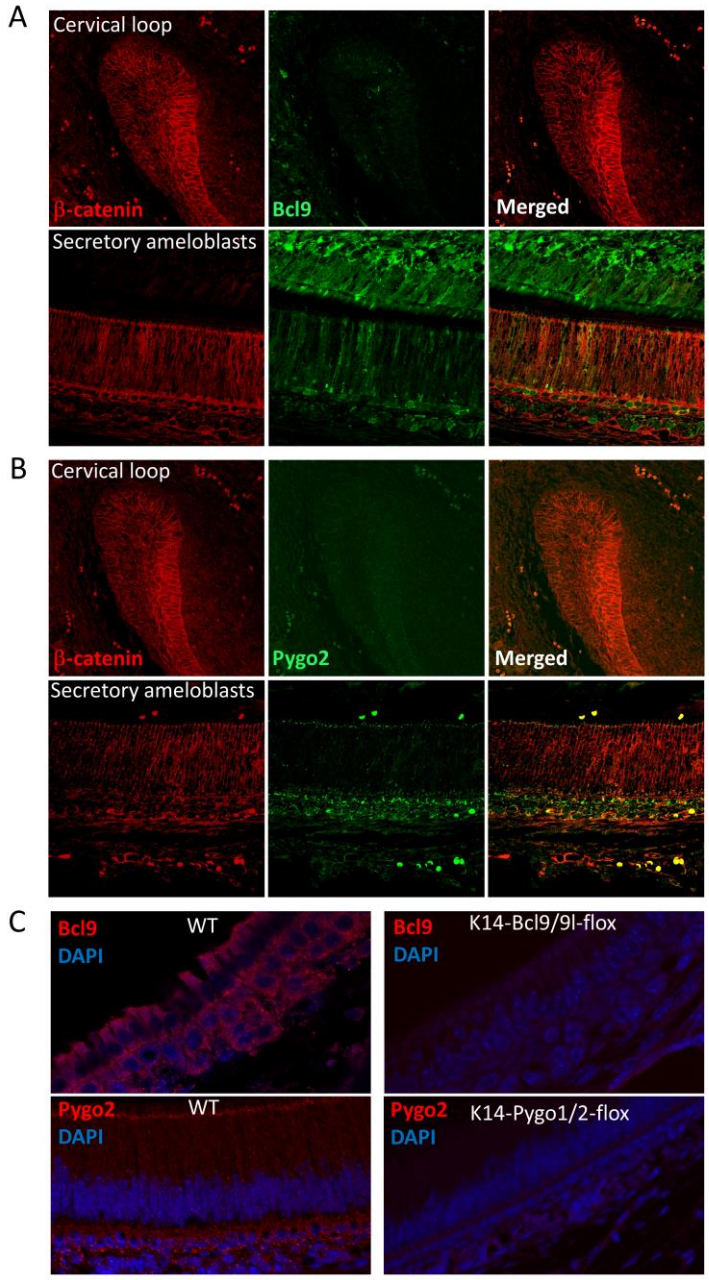

Fig. S1. Bcl9 and Pygo2 are present in differentiated, secretory ameloblasts but not in the stem cell niche.

Confocal images showing β-catenin in red and Bcl9 (**A**) or Pygo2 (**B**) in green in the ameloblast stem cell niche (cervical loop) and in mature, secretory ameloblasts (**A**). There is no detectable Bcl9 or Pygo2 in the labial cervical loop, which constitutes the stem cell niche. (**C**) No Bcl9 (upper panels) or Pygo2 (lower panels) staining is detectable in K14-Bcl9/9l-flox and K14-Pygo1/2-flox ameloblasts, respectively. Each staining was performed on sections derived from at least 3 different animals.

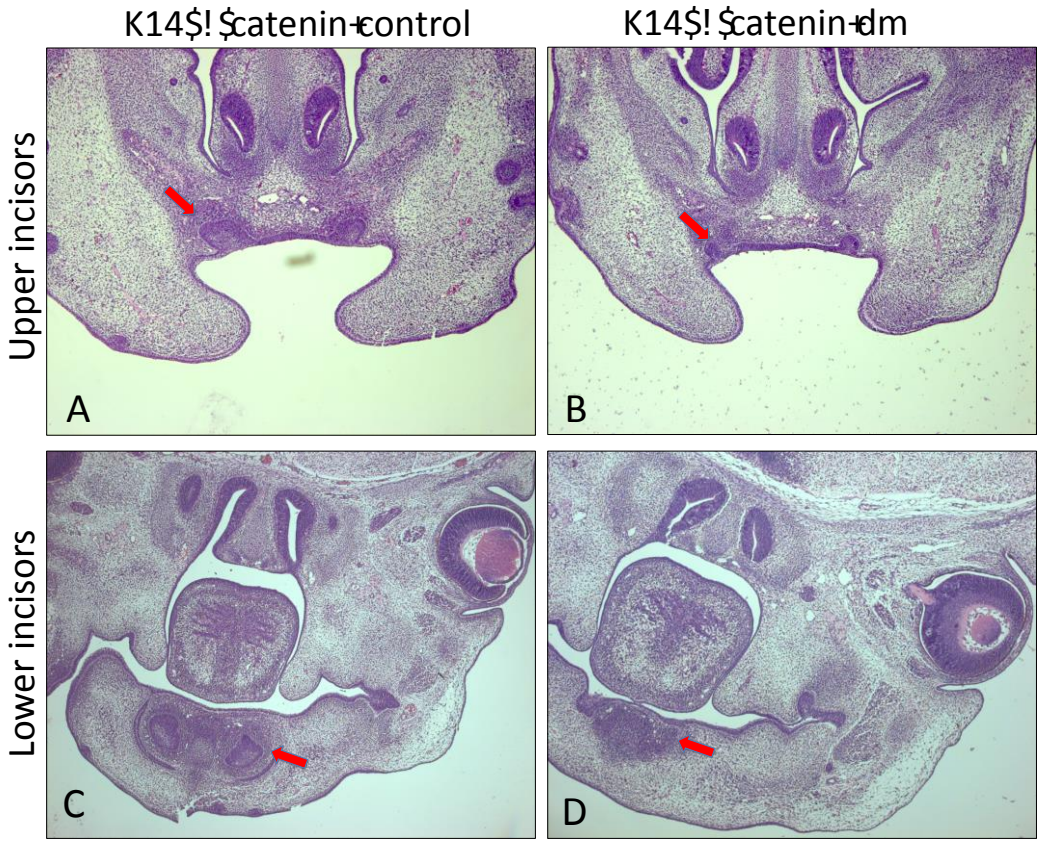

Fig. S2. β-Catenin transcriptional output is required for early tooth development.

Red arrows indicate developing tooth germs of upper (**A, B**) and lower (**C, D**) incisors in control mice and mice lacking transcriptional activity of β-catenin in the oral epithelium (K14-β-cat-dm) at E14.5. In the absence of β-catenin–dependent transcription, tooth development does not proceed beyond the bud stage, N=3.

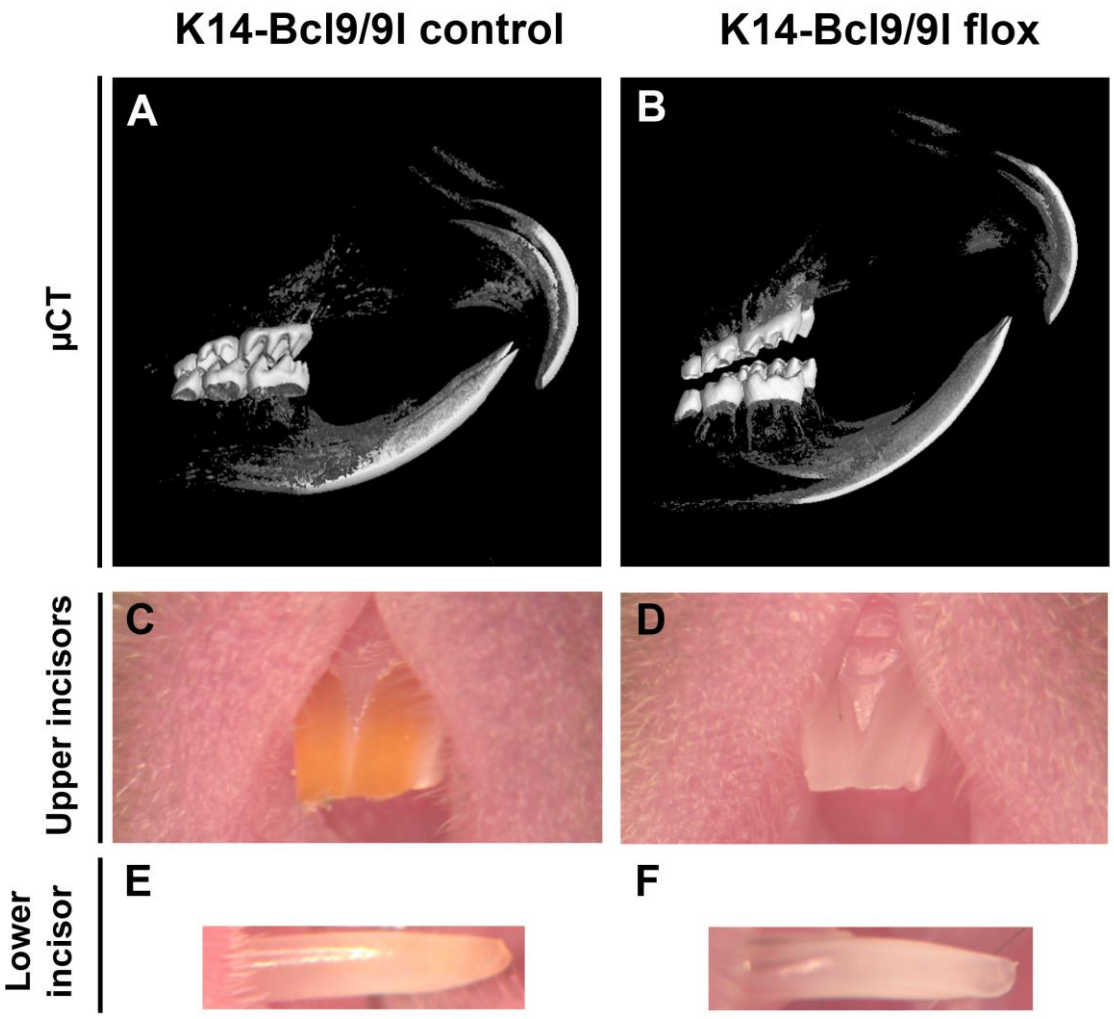

Fig. S3. K14-Cre–mediated deletion of *Bcl9/9l* does not cause early tooth development arrest.

MicroCT analysis of adult heads shows that, as in control mice (**A**), tooth development in K14-Bcl9/9l-flox mice (**B**) proceeds without any obvious morphological alterations. Mutant animals reach adulthood and have functional teeth under laboratory conditions. Whereas teeth from control mice are yellow (**C**, **E**), teeth from *Bcl9*/*Bcl9l* mutant mice (**D**, **F**) are bright white (**D**), N>3.

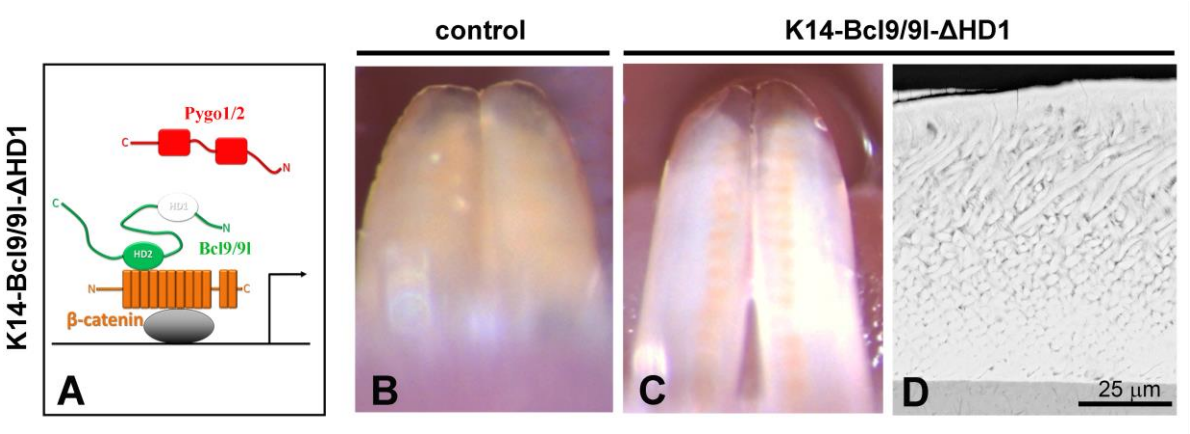

Fig. S4. The Bcl9/9l-Pygo1/2 interaction is required for proper enamel formation.

(**A**) The HD1 domain of Bcl9/9l mediates the interaction between Bcl9/9l and Pygo1/2, and the Bcl9-Pygo complex form in the absence of this domain. (**B, C**) K14-Bcl9/9l-ΔHD1 mice (K14-Cre; *Bcl9*$^{flox/\Delta HD1}$; *Bcl9l*$^{flox/\Delta HD1}$) display a tooth enamel phenotype similar to that of mice lacking Bcl9/9l or Pygo1/2 in the oral epithelium, N>3. (**D**) SEM analysis of tooth enamel from K14-Bcl9/9l-ΔHD1 mice reveals disordering of the hydroxylapatite rods.

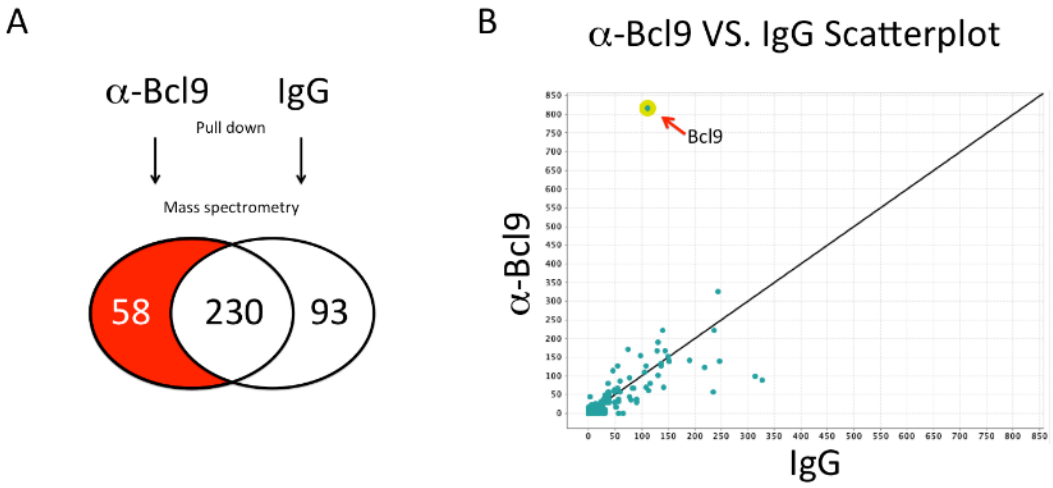

Fig. S5. Ameloblast-specific Bcl9 interactors.

Protein extracts from mouse ameloblasts were subjected to pull-down with an antibody recognizing Bcl9. (**A**) In a representative experiment we consider as potential Bcl9- interacting partners (red) those proteins pulled down by the Bcl9 antibody α-Bcl9 but not by control preimmune serum (IgG). (**B**) Scatterplot showing the proteins differentially pulled down by the two antibodies. The most enriched peptides found with Bcl9 pulldown map to mouse Bcl9 (red arrow), as expected.

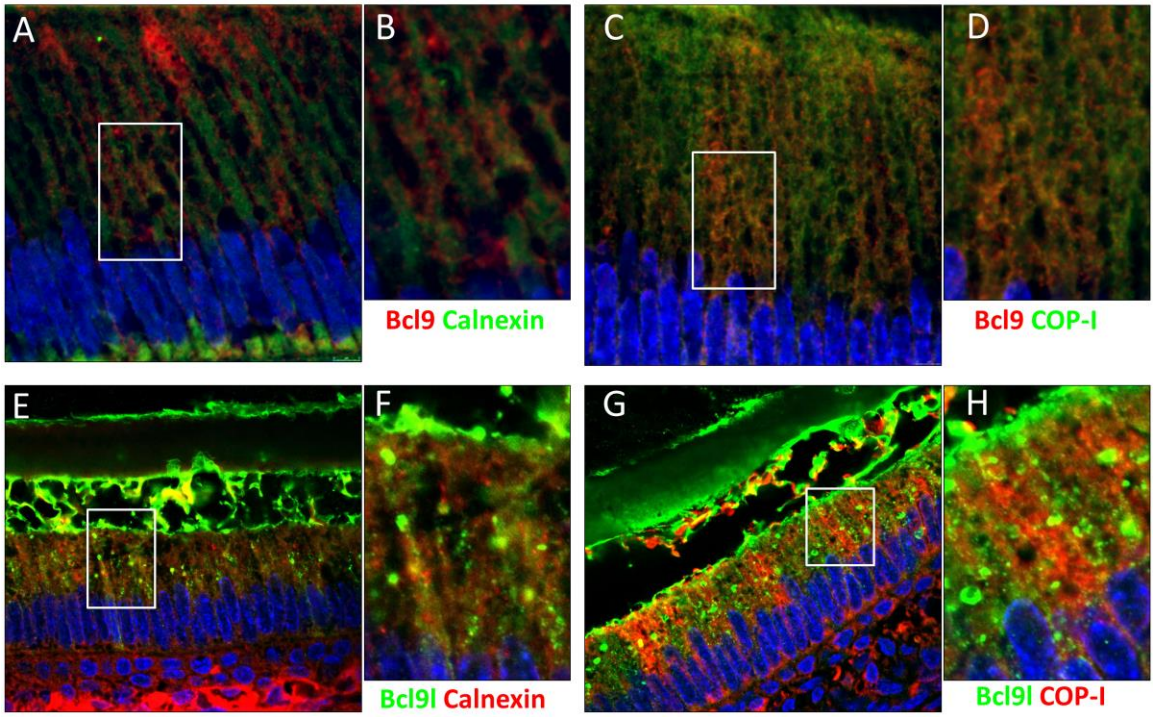

Fig. S6. Bcl9 and Bcl9l are present in the cytoplasm along the secretory pathway.

Confocal immunofluorescence analysis of colocalizatin of Bcl9 (red) with calnexin (green in **A** and **B**) or with COP-I (green in **C** and **D**). (**B**, **D**) Higher magnification of the regions indicated with a white rectangle in **A** and **B**, respectively. As for Bcl9 (Fig. 4D, E)), Bcl9l is also found in association with the two vesicular markers calnexin (**E**, **F**) and COP-I (**G**, **H**), in the cytoplasm. Note the presence of Bcl9l within the enamel, suggesting that Bcl9l is secreted into the extracellular matrix. N=3 different animals for each experiment.

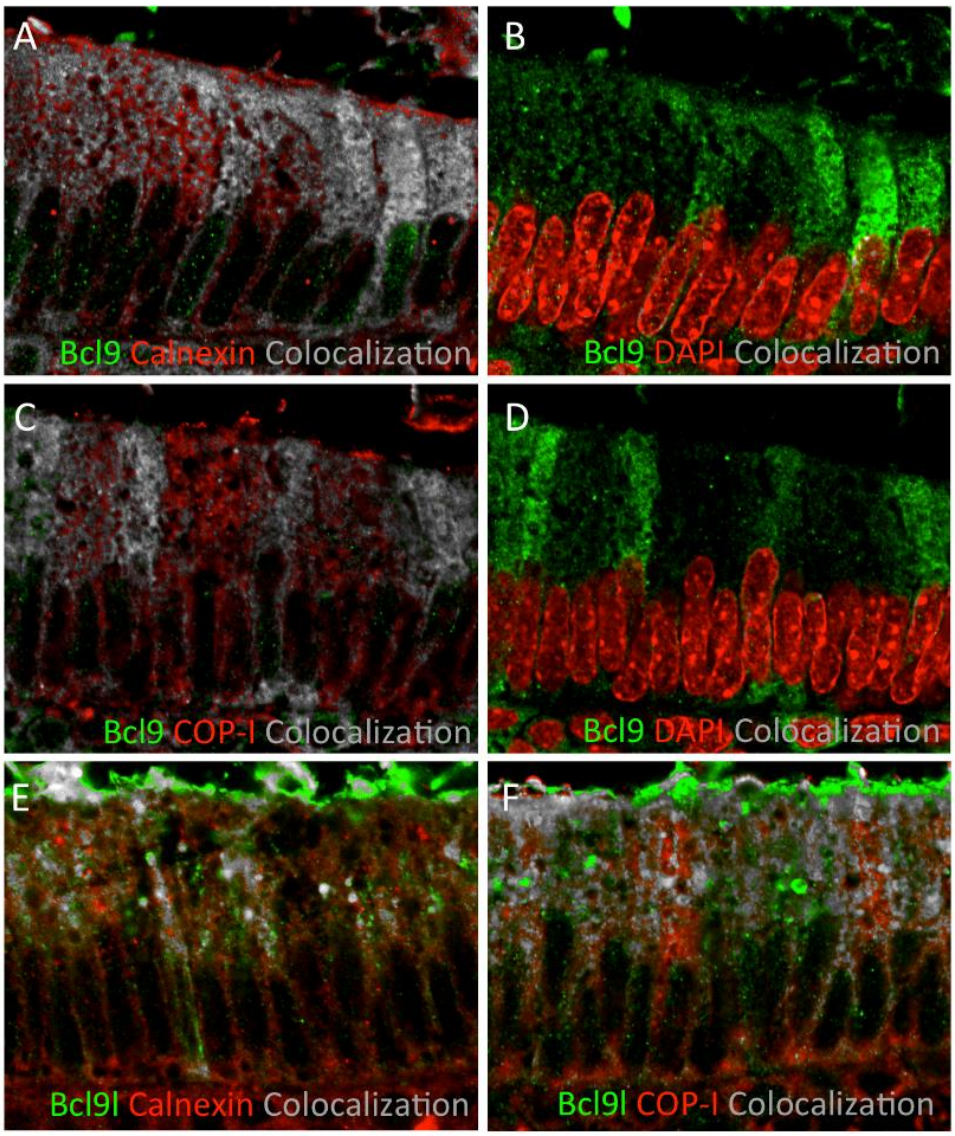

Fig. S7. Bcl9 and Bcl9l colocalize with the secretory pathway proteins calnexin and COP-I.

(**A-F**) Colocalization analyses of Bcl9 with calnexin, COP-I, and the nuclear marker DAPI. Representative confocal immunofluorescence images show Bcl9 in green with calnexin (**A, E**), DAPI (**B, D**), or COP-I (**C, F**) in red. Grey represents the regions of signal colocalization. Note in **B** and **D** the absence of overlapping signal between Bcl9 molecules and DAPI, confirming that Bcl9 is prevalently cytoplasmatic. N=3 different animals for each experiment.

Table S1. Proteins found in two independent pulldown experiments using an antibody recognizing Bcl9 and subtracting the proteins retrieved by pulldown with control preimmune IgG.

Accession	Protein Name
E9Q7G0_MOUSE	Protein Numa1 OS=Mus musculus GN=Numa1 PE=1 SV=1
PPBT_MOUSE	Alkaline phosphatase, tissue-nonspecific isozyme OS=Mus musculus GN=Alpl PE=1 SV=2
HNRL2_MOUSE	Heterogeneous nuclear ribonucleoprotein U-like protein 2 OS=Mus musculus GN=Hnrnpul2 PE=1 SV=2
FBRL_MOUSE	rRNA 2'-O-methyltransferase fibrillarin OS=Mus musculus GN=Fbl PE=2 SV=2
RMXL1_MOUSE	RNA binding motif protein, X-linked-like-1 OS=Mus musculus GN=Rbmxl1 PE=1 SV=1
SFPQ_MOUSE	Splicing factor, proline- and glutamine-rich OS=Mus musculus GN=Sfpq PE=1 SV=1
FUBP2_MOUSE	Far upstream element-binding protein 2 OS=Mus musculus GN=Khsrp PE=1 SV=2
Q8VHM5_MOUSE	Heterogeneous nuclear ribonucleoprotein R OS=Mus musculus GN=Hnrnpr PE=1 SV=1
H2B3B_MOUSE	Histone H2B type 3-B OS=Mus musculus GN=Hist3h2bb PE=1 SV=3
U5S1_MOUSE	116 kDa U5 small nuclear ribonucleoprotein component OS=Mus musculus GN=Eftud2 PE=2 SV=1
FUS_MOUSE	RNA-binding protein FUS OS=Mus musculus GN=Fus PE=2 SV=1
Q9CQM8_MOUSE	60S ribosomal protein L21 OS=Mus musculus GN=Rpl21 PE=2 SV=1
ECHB_MOUSE	Trifunctional enzyme subunit beta, mitochondrial OS=Mus musculus GN=Hadhb PE=1 SV=1
TPM3_MOUSE	Isoform 2 of Tropomyosin alpha-3 chain OS=Mus musculus GN=Tpm3
RS7_MOUSE	40S ribosomal protein S7 OS=Mus musculus GN=Rps7 PE=2 SV=1
RL9_MOUSE	60S ribosomal protein L9 OS=Mus musculus GN=Rpl9 PE=1 SV=2
SND1_MOUSE	Staphylococcal nuclease domain-containing protein 1 OS=Mus musculus GN=Snd1 PE=1 SV=1
RPN1_MOUSE	Dolichyl-diphosphooligosaccharide--protein glycosyltransferase subunit 1 OS=Mus musculus GN=Rpn1 PE=1 SV=1
LUM_MOUSE	Lumican OS=Mus musculus GN=Lum PE=1 SV=2
PRDX4_MOUSE	Peroxiredoxin-4 OS=Mus musculus GN=Prdx4 PE=1 SV=1
PPIA_MOUSE	Peptidyl-prolyl cis-trans isomerase A OS=Mus musculus GN=Ppia PE=1 SV=2
ANXA1_MOUSE	Annexin A1 OS=Mus musculus GN=Anxa1 PE=1 SV=2
BAF_MOUSE	Barrier-to-autointegration factor OS=Mus musculus GN=Banf1 PE=1 SV=1
P63_MOUSE	Tumor protein 63 OS=Mus musculus GN=Tp63 PE=1 SV=1
B1AWE0_MOUSE	Clathrin light chain A OS=Mus musculus GN=Clta PE=1 SV=1
MPCP_MOUSE	Phosphate carrier protein, mitochondrial OS=Mus musculus GN=Slc25a3 PE=1 SV=1
ANXA6_MOUSE	Annexin A6 OS=Mus musculus GN=Anxa6 PE=1 SV=3
PCBP1_MOUSE	Poly(rC)-binding protein 1 OS=Mus musculus GN=Pcbp1 PE=1 SV=1
RL27A_MOUSE	60S ribosomal protein L27a OS=Mus musculus GN=Rpl27a PE=2 SV=5
RL5_MOUSE	60S ribosomal protein L5 OS=Mus musculus GN=Rpl5 PE=1 SV=3
P5CR2_MOUSE	Pyrroline-5-carboxylate reductase 2 OS=Mus musculus GN=Pycr2 PE=2 SV=1
O88375_MOUSE	Keratin associated protein 13 OS=Mus musculus GN=Krtap13 PE=2 SV=1
GSTP1_MOUSE	Glutathione S-transferase P 1 OS=Mus musculus GN=Gstp1 PE=1 SV=2
HUTH_MOUSE	Histidine ammonia-lyase OS=Mus musculus GN=Hal PE=1 SV=1
SMD1_MOUSE	Small nuclear ribonucleoprotein Sm D1 OS=Mus musculus GN=Snrpd1 PE=2 SV=1
PITX2_MOUSE	Isoform Ptx2C of Pituitary homeobox 2 OS=Mus musculus GN=Pitx2
GSDMA_MOUSE	Gasdermin-A OS=Mus musculus GN=Gsdma PE=2 SV=1
TXND5_MOUSE	Thioredoxin domain-containing protein 5 OS=Mus musculus GN=Txndc5 PE=1 SV=2
NUCKS_MOUSE	Nuclear ubiquitous casein and cyclin-dependent kinase substrate 1 OS=Mus musculus GN=Nucks1 PE=1 SV=1
A6ZI44_MOUSE	Fructose-bisphosphate aldolase OS=Mus musculus GN=Aldoa PE=2 SV=1
ENOA_MOUSE	Alpha-enolase OS=Mus musculus GN=Eno1 PE=1 SV=3
K2C72_MOUSE	Keratin, type II cytoskeletal 72 OS=Mus musculus GN=Krt72 PE=3 SV=1
PFKAM_MOUSE	ATP-dependent 6-phosphofructokinase, muscle type OS=Mus musculus GN=Pfkm PE=1 SV=3
TPM2_MOUSE	Isoform 2 of Tropomyosin beta chain OS=Mus musculus GN=Tpm2
A2AIM4_MOUSE	Tropomyosin beta chain OS=Mus musculus GN=Tpm2 PE=3 SV=1
E9Q450_MOUSE	Tropomyosin alpha-1 chain OS=Mus musculus GN=Tpm1 PE=3 SV=1
D3Z724_MOUSE	Protein Gm5965 OS=Mus musculus GN=Gm5965 PE=4 SV=1
MYH4_MOUSE	Myosin-4 OS=Mus musculus GN=Myh4 PE=1 SV=1
Q9D6T8_MOUSE	MCG128973 OS=Mus musculus GN=2310057N15Rik PE=2 SV=1

TERA_MOUSE	Transitional endoplasmic reticulum ATPase OS=Mus musculus GN=Vcp PE=1 SV=4
PRDX1_MOUSE	Peroxiredoxin-1 OS=Mus musculus GN=Prdx1 PE=1 SV=1
AMELX_MOUSE	Amelogenin, X isoform OS=Mus musculus GN=Amelx PE=2 SV=1
PRDX1_MOUSE	Peroxiredoxin-1 OS=Mus musculus GN=Prdx1 PE=1 SV=1
TXND5_MOUSE	Thioredoxin domain-containing protein 5 OS=Mus musculus GN=Txndc5 PE=1 SV=2
A6ZI44_MOUSE	Fructose-bisphosphate aldolase OS=Mus musculus GN=Aldoa PE=2 SV=1
ENOA_MOUSE	Alpha-enolase OS=Mus musculus GN=Eno1 PE=1 SV=3
PFKAM_MOUSE	ATP-dependent 6-phosphofructokinase, muscle type OS=Mus musculus GN=Pfkm PE=1 SV=3